Upregulation of MTHFD2 is associated with PD-L1 activation in bladder cancer via the PI3K/AKT pathway

XINXI DENG[1,2*], XIAOQIANG LIU[1*], BING HU[1], JIANYUN LIU[3], BIN FU[1] and WENSHENG ZHANG[2]

[1]Department of Urology, The First Affiliated Hospital of Nanchang University, Jiangxi Institute of Urology, Nanchang, Jiangxi 330006; [2]Department of Urology, Jiujiang No. 1 People's Hospital (Affiliated Jiujiang Hospital of Nanchang University); [3]Jiangxi Provincial Key Lab of System Biomedicine, Jiujiang University, Jiujiang, Jiangxi 332000, P.R. China

Received August 11, 2022; Accepted December 5, 2022

DOI: 10.3892/ijmm.2022.5217

Abstract. Methylenetetrahydrofolate dehydrogenase 2 (MTHFD2) has been implicated in the etiology of various human malignant tumors; however, its exact role in bladder cancer (BC) remains to be explored. Through reverse transcription-quantitative PCR, western blotting and immunohistochemistry detection of BC tissue, combined with The Cancer Genome Atlas (TCGA) database analysis, the present study demonstrated that MTHFD2 was upregulated in BC tissues. MTHFD2 expression in patients with BC was frequently associated with worse prognosis, tumor immune cell infiltration and programmed death-ligand 1 (PD-L1) expression. Subsequently, using short hairpin RNA, the expression levels of MTHFD2 were knocked down in BC cell lines, and the results revealed that the tumor cell proliferation and colony formation abilities of cells were greatly reduced, as determined by Cell Counting Kit 8 and colony formation assays, as was the expression of PD-L1, as determined by western blotting. These findings were also confirmed in a xenograft nude mouse model. Simultaneously, it was revealed that abnormal expression of MTHFD2 was closely associated with the PI3K/AKT signaling pathway in both RNA-sequencing and TCGA datasets. This observation was verified *in vitro* by detecting the protein expression levels of PI3K and AKT by western blotting. The activation of PI3K and AKT was enhanced in BC cells (T24) following stimulation with 740Y-P, a PI3K activator, and cellular activities and PD-L1 expression levels were restored. Finally, it was demonstrated that the MTHFD2 levels were correlated with chemosensitivity to traditional BC chemotherapeutic agents and various PI3K/AKT-targeted drugs, as determined by analyzing the Genomics of Drug Sensitivity in Cancer database. Overall, the present findings revealed that upregulation of MTHFD2 was associated with PD-L1 activation in BC via the PI3K/AKT signaling pathway, suggesting that it could be a promising marker of chemotherapy and immunotherapy for BC.

Correspondence to: Dr Bin Fu, Department of Urology, The First Affiliated Hospital of Nanchang University, Jiangxi Institute of Urology, 17 Yong Wai Zheng Street, Donghu, Nanchang, Jiangxi 330006, P.R. China
E-mail: urofubin@sina.com

Dr Wensheng Zhang, Department of Urology, Jiujiang No. 1 People's Hospital (Affiliated Jiujiang Hospital of Nanchang University), 48 Taling South Road, Xunyang, Jiujiang, Jiangxi 332000, P.R. China
E-mail: zws971058@163.com

*Contributed equally

Key words: bladder cancer, methylenetetrahydrofolate dehydrogenase 2, immune infiltration, programmed death-ligand 1, PI3K/AKT pathway

Introduction

Bladder cancer (BC) is the sixth most prevalent type of cancer and the ninth most common cause of cancer mortality in men, with an estimated 573,000 new cases and 213,000 mortalities associated with BC worldwide in 2020 (1). Although the current therapeutic strategies for non-muscular invasive BC are acceptable, there is a lack of efficient treatment modalities and predictive markers for advanced BC, which results in poor patient prognosis (2). In addition to surgery, cisplatin-based and neoadjuvant chemotherapy are the main treatment choices for advanced BC (3). Immune checkpoint therapy, which targets proteins including programmed death-1 (PD-1), programmed death ligand-1 (PD-L1) and cytotoxic T-lymphocyte-associated protein 4 (CTLA4), has emerged as a promising treatment for BC in recent years. With therapeutic benefit, PD-1 and PD-L1 inhibitors have been used as a second-line treatment for patients with unresectable and metastatic BC, as well as a first-line treatment for patients with platinum-ineligible and PD-L1-positive BC (4,5). However, similar to other cancer types, only a small percentage of individuals may benefit from this treatment (6). To anticipate the response and increase the efficacy of therapies for advanced BC, further in-depth research on new therapeutic targets and biomarkers is required.

Methylenetetrahydrofolate dehydrogenase 2 (MTHFD2) is a crucial enzyme in folate metabolism that was identified by Mejia and MacKenzie in 1985 (7). MTHFD2 has a dual role as a methylenetetrahydrofolate dehydrogenase and as a methylenetetrahydrofolate cyclohydrolase, and is important for cell proliferation and viability (7). MTHFD2 efficiently drives the

folate cycle in embryonic tissue to supply the high nucleotide requirement needed for cell proliferation. It has also been reported to be increased in numerous types of cancer where it enhances cell proliferation by fulfilling the high biosynthetic demand; by contrast, MTHFD2 depletion may impair aggressive characteristics and trigger cell death in a variety of malignancies (8). As a result of its specific expression pattern and prognostic importance, MTHFD2 has attracted increased interest in cancer research (9-13). MTHFD2 has been shown to induce carcinogenesis in breast cancer via activating the AKT signaling pathway (14), and it may promote cell proliferation, migration and cell cycle entry, while also suppressing apoptosis in colorectal cancer cell lines (15). Furthermore, MTHFD2 may promote lung adenocarcinogenesis and metastasis through activating the AKT/GSK-3β/β-catenin signaling pathway (16). In BC, MTHFD2 can promote cell proliferation by activating CDK2 (17), and it has been reported to be strongly associated with poor prognosis and a high level of immune infiltrates, according to a previous bioinformatics study (18). However, its specific role in BC remains to be explored.

The present study used a combination of bioinformatics analysis and experimental validation to systematically investigate the expression, function and molecular mechanisms of MTHFD2 in BC. In addition, the present study analyzed the association between the expression of MTHFD2 and patient prognosis, immune infiltration and PD-L1 expression. The present study aimed to determine whether MTHFD2 may be considered a promising marker and therapeutic target of chemotherapy and immunotherapy for BC.

Materials and methods

Specimens. A total of 24 pairs of BC and adjacent tissues were obtained from the Department of Urology, The First Affiliated Hospital of Nanchang University (Nanchang, China) with ethics approval. The patients were aged between 45 and 80 years, with a median age of 74 years. The male to female ratio was 5:1. All specimens were included in this study after confirmation by two senior pathologists. Those samples were collected between March 2015 and January 2017 after transurethral resection of bladder tumors or radical cystectomy, and all of the specimens were confirmed by pathology. The present study was approved by the Ethics Committee of The First Affiliated Hospital of Nanchang University [approval no. (2021)51]. In addition, a tissue microarray (TMA) including 63 BC tissues and 16 paired adjacent tissues was purchased from Shanghai Outdo Biotechnology Co., Ltd. Three pairs of samples failed to detect results. The TMA (cat. no. HBlaU079Su01) contained information regarding patient outcomes (median follow-up time, 25.5 months), basic pathological information of the patients, and immunohistochemical expression of CD8 and PD-L1. The age of the patients ranged between 42 and 85 years, with a median age of 71 years. The male to female ratio was 5.3:1. The use of the TMA in the present study was approved by the Ethics Committee of The First Affiliated Hospital of Nanchang University [approval no. (2021)51]. The TMA was used to perform IHC analysis of MTHFD2.

Lentiviral construction. A packaging lentivirus (pHBLV-U6-MCS-CMV-ZsGreen-PGK-PURO) was purchased from Hanheng Biotechnology (Shanghai) Co., Ltd. The sequences of shRNAs targeting the mRNA sequence of MTHFD2 and the scrambled control NC were as follows: MTHFD2 shRNA1, 5'-CGAATG TGTTTGGATCAGTAT-3'; MTHFD2 shRNA2, 5'-GCAGTT GAAGAAACATACAAT-3'; MTHFD2 shRNA3, 5'-CGA GAAGTGCTGAAGTCTAAA-3'; NC shRNA, 5'-TTCTCC GAACGTGTCACGTAA-3'. These shRNA sequences were subcloned into the lentivirus vector (pHBLV-U6-MCS-CMV -ZsGreen-PGK-PURO). Briefly, the expression vectors were co-transfected with packaging plasmid psPAX2 (Addgene, Inc.) and envelope plasmid pMD2.G (Addgene, Inc.) into 293T cells (American Type Culture Collection) using a second generation system, according to the manufacturer's protocols [10 μg pSPAX2, 5 μg pMD2G, 10 μg plasmid and 75 μl Lipofiter™ (cat. no. HB-TRLF-1000; Hanheng Biotechnology Co., Ltd.)]. After transfection for 48 h at 37˚C, infectious particles were harvested and filtered using 0.45-mm cellulose acetate filters, concentrated by ultracentrifugation and stored at -80˚C.

The T24 and UMUC3 BC cell lines were infected with lentiviral knockdown MTHFD2 (HBLV-h-MTHFD2shRNA1/2/3-ZsGreen-PURO) or NC (HBLV-ZsGreen-PURO) constructs using the one-half volume infection method according to the manufacturer's protocols. Cells were seeded in 6-well plates at a density of $1x10^5$ cells/well. After an overnight incubation, cell culture medium was exchanged with one-half volume fresh medium containing Polybrene (4 μg/ml) and lentiviral solution (the virus solution volume was calculated as V=cell number x MOI/virus titer, MOI=10). A total of 4 h after infection, another one-half of fresh medium was added. Infection efficiency of cells was observed under a fluorescence microscope after 24 h. The stably infected cell lines were screened with puromycin (2 μg/ml). When the transduction efficiency was >90%, stable cell lines were used in subsequent experiments.

Bioinformatics analysis

Data acquisition and processing. Open-access mRNA expression data and clinical information of patients with BC were downloaded from The Cancer Genome Atlas (TCGA) database (https://portal.gdc.cancer.gov/; TCGA-BC). RNA-sequencing (RNA-seq) data and clinical information were obtained from 414 patients (tumor samples, n=414; normal samples, n=19). Before analysis, data were preprocessed and normalized as previously described (19).

Immune cell infiltration analysis. TIMER (https://cistrome.shinyapps.io/timer/) is a web server that analyzes tumor-infiltrating immune cells based on TCGA data (20). In the present study, TIMER was utilized to investigate the pan-cancer expression of MTHFD2, as well as the association between MTHFD2 expression and immune cell infiltration or immune checkpoint expression in BC. CIBERSORT deconvolution (https://cibersort.stanford.edu/) was used to estimate 22 different cell types for immune infiltration analyses. To calculate ESTIMATE-score, immune-score and stromal-score for TCGA-BC data, the ESTIMATE algorithm (Verhaak Lab; http://bioinformatics.mdanderson.org/estimate) was used.

Identification of differentially expressed genes (DEGs). The 'limma' package in R software (https://bioconductor.

org/packages/limma/) was used to study the DEGs. For TCGA-BC data, 'adjusted P<0.05 and fold-change (FC)>2' were defined as the threshold for the differential expression of mRNA between normal and BC samples, whereas for RNA-seq (T24-shRNA2 vs. T24-NC) data, 'adjusted P<0.05 and FC>1.5' were defined as the threshold for the differential expression of mRNA. Pheatmap package (version 1.0.12, https://cran.r-project.org/web/packages/pheatmap/index.html) in R was utilized to perform the hierarchical cluster analysis of DEGs between the T24-NC and T24-shRNA2.

Gene Set Enrichment Analysis (GSEA). To better understand the function of MTHFD2 in BC, the biological differences between patients with low/high MTHFD2 expression in TCGA-BC and T24-shRNA2/T24-NC were evaluated by GSEA in R, using the packages 'fgsea' (https://bioconductor.org/packages/fgsea) and 'clusterProfiler' (https://bioconductor.org/packages/clusterProfiler/) respectively. The reference pathway lists used were Gene Ontology (GO), Kyoto Encyclopedia of Genes and Genomes (KEGG) and Hallmark (version 7.5.1; https://www.gsea-msigdb.org). R software Gene Set Variation Analysis (GSVA) package (https://bioconductor.org/packages/release/bioc/html/GSVA.html) was used to analyze the correlation between MTHFD2 expression and pathway activation by choosing 'ssgsea' parameter. The correlation between genes and pathway scores was analyzed by Spearman correlation. Genes in enriched biological pathways were selected and Cytoscape version 3.8.1 was used for graphical representations of the pathways (21).

Drug sensitivity analysis. The chemotherapeutic response for each sample of TCGA-BC dataset was predicted based on the largest publicly available pharmacogenomics database, namely the Genomics of Drug Sensitivity in Cancer (GDSC; https://www.cancerrxgene.org/). The prediction process was implemented by the R package 'pRRophetic' (https://github.com/paulgeeleher/pRRophetic). The half-maximal inhibitory concentration (IC_{50}) of the samples was estimated by ridge regression. All parameters were set as default values. Using the batch effect correction package 'ComBat' in R software (https://rdrr.io/bioc/sva/man/ComBat.html)and the type of all tissues, duplicate gene expression was summarized as the mean value.

Cell culture. Human BC cell lines, including UMUC3, T24, 5637 and J82, and the SV-HUC-1 (human bladder cell biochemistry Pillon) cell line were purchased from The Cell Bank of Type Culture Collection of Chinese Academy of Sciences. T24 cells were cultured in high-glucose DMEM (Gibco; Thermo Fisher Scientific, Inc.). UMUC3 and J82 cells were cultured in MEM (Gibco; Thermo Fisher Scientific, Inc.). 5637 cells were cultured in 1640 medium (Gibco; Thermo Fisher Scientific, Inc.). SV-HUC-1 cells were cultured in F12k medium (Gibco; Thermo Fisher Scientific, Inc.). All culture media contained 10% fetal bovine serum (FBS; HyClone; Cytiva), 100 U/ml penicillin and 100 μg/ml streptomycin. T24 and T24-shRNA2 cells were stimulated with DMSO or 90 μg/ml 740 Y-P (TargetMol) for 48 h at 37˚C in order to confirm that MTHFD2 regulates the proliferation of BC cells and PD-L1 expression via the PI3K/AKT pathway. All of the cells were cultured at 37˚C in an atmosphere containing 5% CO_2.

Western blot analysis. Total proteins were extracted from T24 and UMUC3 cells or preserved BC and adjacent tissues, and were stored at -80˚C. Western blot analysis was performed as previously described (22). Total proteins were isolated using RIPA lysis buffer (Beyotime Institute of Biotechnology) and were quantified using a BCA protein Assay kit (Thermo Fisher Scientific, Inc.). Proteins (20 μg/lane) were separated by SDS-PAGE on 12% gels and transferred to PVDF membranes. After blocking for 2 h with 5% skimmed milk at room temperature, the membranes were incubated with diluted primary antibodies overnight at 4˚C. The primary antibodies and concentrations used in the present study were as follows: β-actin (cat. no. 58169; 1:1,000; Cell Signaling Technology, Inc.), MTHFD2 (cat. no. 98116; 1:1,000; Cell Signaling Technology, Inc.), anti-phosphorylated (p)-PI3K (cat. no. 17366; 1:1,000; Cell Signaling Technology, Inc.), anti-p-AKT (cat. no. 4060; 1:1,000; Cell Signaling Technology, Inc.), anti-PI3K (cat. no. 4257; 1:1,000; Cell Signaling Technology, Inc.), anti-AKT (cat. no. 4691; 1:1,000; Cell Signaling Technology, Inc.) and anti-PD-L1 (cat. no. ab282458; 1:1,000; Abcam). Subsequently, the membranes were incubated with a horseradish peroxidase-labeled goat anti-rabbit secondary antibody (cat. no. ab6721; 1:3,000; Abcam) or goat anti-mouse (cat. no. ab6789; 1:3,000; Abcam) for 1.5 h at room temperature. BeyoECL Plus (Beyotime Institute of Biotechnology) was used to visualize the protein bands. ImageJ 1.45 software (National Institutes of Health) was used to perform densitometric analysis of each band.

Hematoxylin and eosin (H&E) staining and immunohistochemistry (IHC). Tumor tissue from nude mice, or BC and adjacent nontumor tissues from the TMA were fixed with 4% neutral formaldehyde for <24 h at room temperature, rehydrated in a graded alcohol series, rendered transparent with xylene, embedded in paraffin and sectioned (4 μm). The TMA was manufactured by Shanghai Outdo Biotechnology Co., Ltd. Subsequently, antigen retrieval was performed with Tris-EDTA (pH 9.0) for 15 min in a microwave. The sections were then incubated at 37˚C in 3% H_2O_2 for 10 min and blocked in 10% sheep serum (Shanghai Yaji Biotechnology Co., Ltd.) for 10 min. The tissues were incubated with a primary antibody against MTHFD2 (cat. no. ab151447; 1:200; Abcam) or PD-L1 (cat. no. ab282458; 1:500; Abcam) overnight at 4˚C, followed by incubation with a secondary antibody (cat. no. ab288151; 1:200; Abcam) for 30 min at room temperature and staining with DAB (Dako; Agilent Technologies, Inc.). Slides were then stained with hematoxylin for 5 min at room temperature and sealed with neutral gum. For H&E staining, the sections were stained with hematoxylin for 3 min and eosin for 1 min at room temperature. Images was captured under a light microscope. Images of the TMA were scanned using a Pannoramic SCAN II (3DHISTECH Ltd.) and analyzed using Quant Center 2.1 software (3DHISTECH Ltd.).

The cytoplasmic staining results were evaluated by two independent pathologists based on the percentage of positive cells and the intensity of staining. The intensity of staining was scored as 0, no staining; 1, mild staining; or 2, deep staining. The percentage of positive cells was scored as: 0, no tumor cells stained; 1, <10% tumor cells stained; 2, 10-50% tumor cells stained; and 3, >50% tumor cells stained. The

results were calculated as 'intensity x proportion'. A total score of <2 was defined as negative expression, whereas ≥2 was defined as positive expression. ImageJ 1.45 software (National Institutes of Health) was used to determine mean protein expression for IHC.

RNA extraction and reverse transcription-quantitative PCR (RT-qPCR). Total RNA was extracted from UMUC3, T24, 5637, J82 and SV-HUC-1 cells and tissues using TRIzol® reagent (Invitrogen; Thermo Fisher Scientific, Inc.), and the concentration and purity of the extracted RNA were assessed according to the optical density (OD)260/OD280 value. cDNA was synthesized using a Takara PrimeScript RT reagent kit (cat. no. RR037A; Takara Bio, Inc.) according to the manufacturer's protocol. qPCR was performed using SYBR Premix EX Taq kit (Takara Bio, Inc.) under the following thermocycling conditions: Initial denaturation at 95˚C for 30 sec, followed by 40 cycles at 95˚C for 5 sec and 60˚C for 30 sec for annealing and elongation. β-actin was used as the internal reference gene (22). The mRNA relative expression levels were evaluated using the $2^{-\Delta\Delta Cq}$ method (23). The primer sequences were as follows: β-actin, forward 5'-TCTCCCAAGTCCACACAGG-3', reverse 5'-GGCACGAAGGCTCATCA-3'; and MTHFD2, forward 5'-CAGCAGATCAAGCAGGAAG-3', reverse 5'-GCAGGATTCTCGCCAAC-3'.

Cell Counting Kit-8 (CCK-8) assay. The CCK-8 assay was performed to measure cell viability. Briefly, ~1x10^3 UMUC3 or T24 cells were seeded into 96-well plates and cultured for 24 h. Subsequently, 10 μl CCK-8 solution (Nanjing KeyGen Biotech Co., Ltd.) was added to each well at 0, 24, 48 and 72 h. After incubation for 2 h, the absorbance was measured at 450 nm with a Spark™ 10 M microplate reader (Tecan Group, Ltd.).

Apoptosis and cell cycle analysis. For the analysis of apoptosis and cell cycle distribution, ~1x10^6 UMUC3 or T24 cells were collected and washed twice in pre-cooled PBS. For apoptosis analysis, 7-aminoactinomycin D (7-AAD) and annexin V-allophycocyanin (APC) solutions were added for 15 min at 4˚C, according to the instructions of the manufacturer of the apoptosis kit (cat. no. AP105-100; Hangzhou Lian Ke Biotechnology Co., Ltd.). For cell cycle analysis, PI and RNase [PI (20X) and RNase A (50X); ratio, 5:2] were added for 10 min at 4˚C according to the manufacturer's instructions (cell cycle kit; cat. no. MA0334; Dalian Meilun Biotechnology Co., Ltd.). Cells were then measured using flow cytometry (Accuri C6; BD Biosciences) and analyzed using FlowJo 10.8.1 (FlowJo LLC).

Colony formation assay. UMUC3 or T24 cells (~300 cells/well for T24 and ~400 cells/well for UMUC3) were seeded in 6-well plates, and cultured in an incubator (37˚C, 5% CO_2) with 10% FBS-containing medium for 10-14 days. The culture was terminated when the number of cells per colony was >50 as observed under a light microscope, or when the colony was visible under the naked eye. Cells were fixed with 4% paraformaldehyde for 30 min at room temperature. The colonies were stained with 0.1% crystal violet for 15 min at room temperature and images were captured. The number of colonies formed was calculated manually.

Tumor formation in nude mice. Female BALB/c nude mice (age, 4 weeks; weight, 30 g) were obtained from Hunan Silaike Jingda Laboratory Animal Co., Ltd. and were housed under a controlled temperature of 22˚C, 50% humidity with a 12-h light/dark cycle, and had *ad libitum* access to food and water. A total of 14 mice were divided into two groups (n=7 mice/group). All animal experimental protocols were approved by the Animal Care and Use Committee of Nanchang University [approval no. SYXK (Gan) 2015-0001]. Briefly, T24-NC and T24-shRNA2 cells at a density of 1x10^8 cells/ml were resuspended in 200 μl Matrigel and were injected subcutaneously into the left flanks of mice. The size of the tumor was recorded every 3-6 days, and the volume was calculated as $V=1/2 \times A \times B^2$ (where A is the longest diameter and B is the shortest diameter). After 4 weeks, the nude mice were euthanized by cervical dislocation, and tumors were photographed, measured, weighed and immunohistochemically stained. Death was confirmed by respiratory arrest. Humane endpoints were used in the present study, including tumor diameter >20 mm, inability to stand, weight loss >20% and failure to response to external stimuli.

RNA-seq. RNA-seq was performed by NovelBio Bio-Pharm Technology Co., Ltd. Total RNA was extracted from three replicates of T24-NC and T24-shRNA2 using TRIzol reagent (Invitrogen; Thermo Fisher Scientific, Inc.). The RNA quality was assessed using an Agilent 2200 (cat. no. G2965AA; Agilent Technologies, Inc.) and stored at -80˚C. cDNA libraries were constructed for each RNA sample using the HiSeq X Ten Reagent kit v2.5 (cat. no. FC-501-2501; Illumina, Inc.) according to the manufacturer's protocol. The libraries were quality controlled and the concentration was measured with Agilent 2200, and sequenced by HiSeq X (cat. no. HiSeq X 10; Illumina, Inc.) on a 150 bp paired-end run. The loading concentration of the final library was 10 pM. The clean reads were then aligned to the human genome (GRCh38; National Center for Biotechnology Information) using Hisat2 (24). HTseq (25) was used to calculate gene counts, while the Reads Per Kilobase per Million mapped reads method was used to determine gene expression.

Statistical analysis. GraphPad Prism 8.00 software (GraphPad Software, Inc.) and R (version 4.0.2, https://www.R-project.org/) were used for data analysis. The Shapiro-Wilk test was used to determine if the data had a normal distribution. Paired Student's t-test was used for expression analysis of paired bladder cancer and adjacent tissues. Unpaired Student's t-test or one-way ANOVA with post hoc Turkey's honest significant difference test were used in the case of other normal distribution. A nonparametric test (Wilcoxon signed-rank or Kruskal-Wallis with Dunn's post hoc test) was used elsewhere. If not otherwise specified, quantitative data are expressed as the mean ± standard deviation. Kaplan-Meier survival curves were plotted using the 'survival' package (https://CRAN.R-project.org/package=survival) in R (version 4.0.2) to analyze the association between MTHFD2 expression and the overall survival (OS) of patients with BC. In the survival analysis, the R package 'maxstat' (maximally selected rank statistics with several P-value approximations version 0.7-25, https://CRAN.R-project.org/package=maxstat) was used to

calculate the optimal cut-off value of MTHFD2 expression, setting the minimum number of grouping samples to be >25%, and the maximum number of samples to be grouped <75%. The best cut-off value was obtained as 12.23408 for TCGA-BC and 0.000844 for TMA. In other analyses, grouped cut-off values were set as the median MTHFD2 expression. Based on such cut-off values, the patients were divided into two groups: High and low MTHFD2 expression. Log-rank test was used to determine P-values. Univariate and multivariate Cox regression analyses were performed to evaluate the OS of patients in TCGA-BC cohort. The correlation between the two variables was calculated by Spearman's rank correlation analysis. $P<0.05$ was considered to indicate a statistically significant difference.

Results

MTHFD2 is highly expressed in BC. The expression of MTHFD2 in pan-cancer was first examined using the TIMER online tool. MTHFD2 was highly expressed in various types of cancer, including Bladder Urothelial Carcinoma (Fig. 1A). In the analysis of TCGA-BC data, an unpaired tissue comparison revealed that MTHFD2 expression was significantly increased in BC, when 414 BC samples were compared with 19 normal bladder tissue samples using RNA-seq (Fig. 1B). Similar results were obtained when the 19 BC samples were compared with their matched normal bladder tissue samples (Fig. 1C). IHC was used to examine the expression of MTHFD2 in BC tumor and normal tissues in a commercial TMA. BC tumor tissues exhibited higher MTHFD2 expression than normal tissues (Fig. 1F). Further analysis of the expression data in the TMA also indicated that MTHFD2 was highly expressed in BC, both when 60 BC samples were compared with 13 unpaired normal bladder tissue samples (Fig. 1D) and when 13 BC samples were compared with their matched normal bladder tissue samples (Fig. 1E). To assess the roles of MTHFD2 in BC cells, the mRNA expression levels of MTHFD2 were detected in SV-HUC-1 cells and in BC cell lines (UMUC3, T24, J82 and 5637) using RT-qPCR. As shown in Fig. 1G, the mRNA expression levels of MTHFD2 were significantly higher in BC cells compared with those in SV-HUC-1 cells. Subsequently, the mRNA expression levels of MTHFD2 were detected in 24 pairs of cancer and adjacent tissues collected at our hospital by RT-qPCR (Fig. 1H), and MTHFD2 protein expression in six pairs of high-grade BC and adjacent tissues was detected by western blotting (Fig. 1I). Both mRNA and protein expression levels of MTHFD2 were significantly higher in BC tissues compared with those in adjacent tissues. MTHFD2 expression was also strongly associated with TNM-T stage (Fig. 2A) and American Joint Committee on Cancer (AJCC) stage (Fig. 2B) in TCGA-BC data. In addition, a similar trend was observed in the TMA data (Fig. 2C and D); however, the results did not reach statistical significance, possibly due to the small sample size of the individual groups. Taken together, these results confirmed that MTHFD2 was highly expressed in BC.

MTHFD2 expression in BC is associated with poor prognosis. The association between MTHFD2 expression and OS was analyzed in patients with BC. Patients with elevated MTHFD2 levels had significantly shorter OS in TCGA-BC cohort (Fig. 2E). A similar result was obtained for the TMA data (Fig. 2F). Subsequently, in the univariate Cox regression analysis, age, AJCC stage, TNM-T stage, TNM-N stage and MTHFD2 expression were significantly associated with the OS of patients with BC (Fig. 2G). Missing values were removed from multivariate Cox regression analysis and the remaining samples were included. In the multivariate Cox regression analysis (Fig. 2H), only age remained a significant and independent factor. The expression of MTHFD2 exhibited a trend to associate with patient OS, but it was not statistically significant, possibly due to the interference of other clinical features.

MTHFD2 expression is associated with immune cell infiltration in BC. The association between MTHFD2 expression and immune cell infiltration in BC was investigated using the TIMER database (Fig. 3A). It was revealed that MTHFD2 was negatively correlated with tumor purity ($r=-0.211$; $P=4.39\times10^{-5}$), and was positively correlated with the infiltration of $CD8^+$ T cells ($r=0.364$; $P=6.38\times10^{-13}$), macrophages ($r=0.145$; $P=5.49\times10^{-3}$), neutrophils ($r=0.269$; $P=2.03\times10^{-7}$) and dendritic cells ($r=0.407$; $P=5.62\times10^{-16}$); however, the correlations with tumor purity, macrophages and neutrophils were weak. Differences in immune infiltration between the low- and high-MTHFD2 expression groups for 22 immune cells were analyzed using CIBERSORT. As shown in Fig. 3B, the distribution of memory B cells ($P=4.78\times10^{-4}$), plasma B cells ($P=1.25\times10^{-4}$), $CD4^+$ naive T cells ($P=2.57\times10^{-4}$), $CD4^+$ memory-activated T cells ($P=7.72\times10^{-12}$), follicular T helper cells ($P=2.53\times10^{-2}$), regulatory T cells ($P=4.20\times10^{-7}$), monocytes ($P=9.10\times10^{-6}$), M0 macrophages ($P=3.78\times10^{-6}$), M1 macrophages ($P=1.16\times10^{-9}$), M2 macrophages ($P=3.95\times10^{-3}$), activated myeloid dendritic cells ($P=2.31\times10^{-5}$), activated mast cells ($P=3.33\times10^{-8}$), resting mast cells ($P=4.21\times10^{-7}$) and neutrophils ($P=2.22\times10^{-2}$) was significantly different between the low- and high-MTHFD2 expression groups. In addition, a correlation was identified between MTHFD2 expression and various immune-related molecules using the TIMER database, including immune-stimulators, immune-inhibitors, major histocompatibility complex (MHC) molecules, chemokines and receptors (Fig. S1). The association between MTHFD2 and immune checkpoint molecules is shown in Fig. 3C. MTHFD2 expression was strongly associated with the expression of CD274 ($P=1.33\times10^{-21}$), CTLA4 ($P=2.80\times10^{-12}$), HAVCR2 ($P=1.39\times10^{-18}$), LAG3 ($P=9.94\times10^{-19}$), PDCD1 ($P=6.29\times10^{-12}$), PDCD1LG2 ($P=1.29\times10^{-22}$), TIGIT ($P=5.76\times10^{-11}$) and SIGLEC15 ($P=3.04\times10^{-22}$). The tumor mutational burden (TMB) has been reported to be helpful in predicting the response to immune checkpoint inhibitor treatment across numerous cancer types (26). A weak positive correlation was identified between TMB and MTHFD2 expression in TCGA-BC cohort ($r=0.21$; $P=2.54\times10^{-5}$; Fig. 3D). As shown in Fig. 3E, the tumor microenvironment (TME)-related scores were compared between the low- and high-MTHFD2 expression groups of TCGA-BC cohort using ESTIMATE. It was observed that samples with high MTHFD2 expression had higher ESTIMATE, immune and stromal scores. Furthermore, using the expression data of CD8 and PD-L1 in the TMA, the correlation between MTHFD2 and CD8/PD-L1 expression in the TMA cohort was verified. The results showed that MTHFD2 expression was weakly positively correlated with

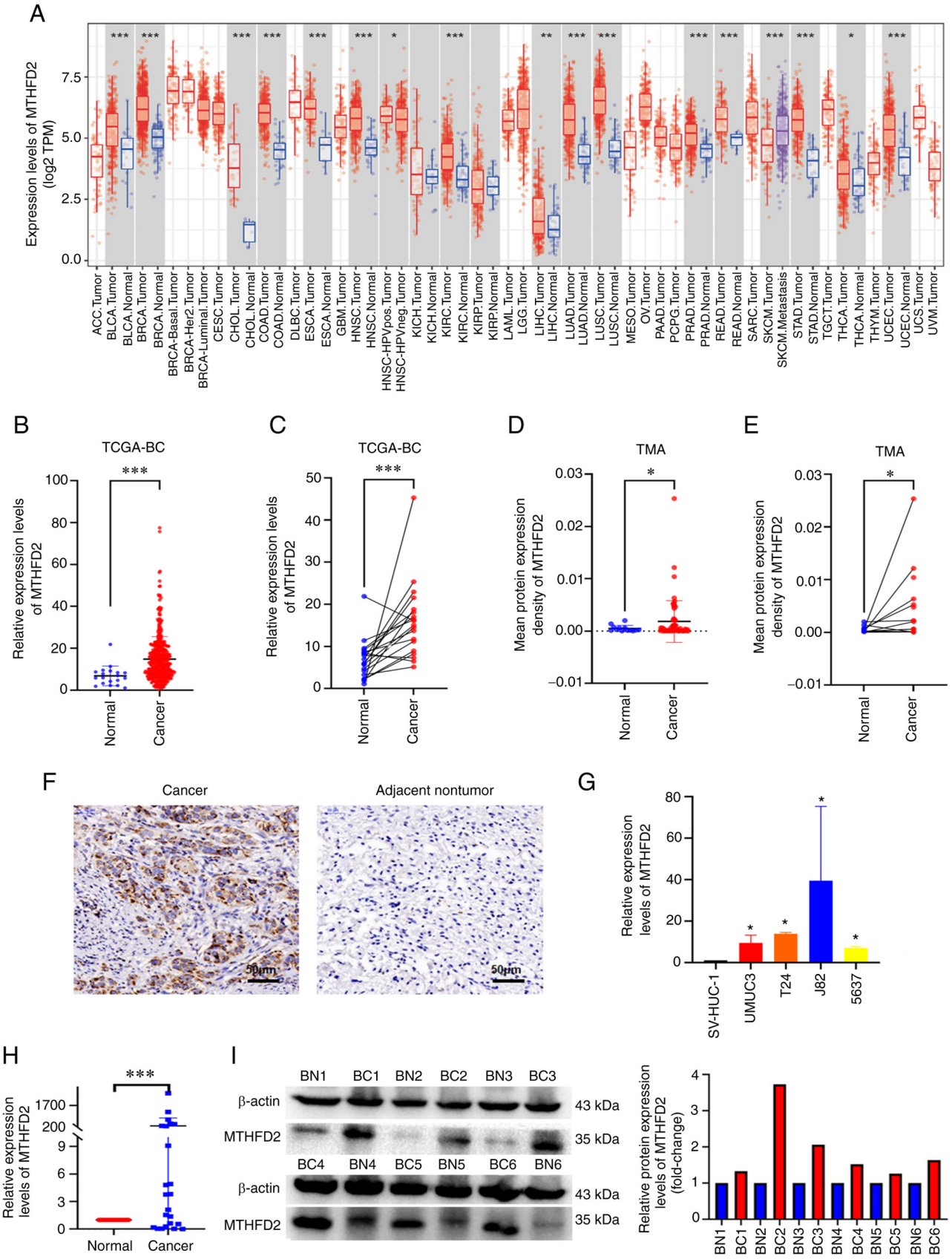

Figure 1. Elevated expression of MTHFD2 in BC. (A) Pan-cancer analysis of MTHFD2 expression, as determined by TIMER. (B) MTHFD2 expression in BC tissue samples and normal bladder tissue samples from TCGA database. (C) MTHFD2 expression in paired BC tissue samples and normal bladder tissue samples from TCGA database. (D) MTHFD2 expression in BC tissue samples and normal bladder tissue samples from the TMA. (E) MTHFD2 expression in paired BC tissue samples and normal bladder tissue samples from TMA. (F) Immunohistochemical analysis of MTHFD2 in the BC tumor and adjacent normal tissues. (G) Expression levels of MTHFD2 in BC and normal bladder cell lines detected by RT-qPCR. (H) Relative expression of MTHFD2 in BC tissues (n=24) and adjacent tissues (n=24) detected by RT-qPCR. (I) Relative expression levels of MTHFD2 in six paired bladder cancer tissues and adjacent tissues detected by western blotting. *P<0.05, **P<0.01, ***P<0.001 as indicated or vs. adjacent tissues or SV-HUC-1 cells. BC, bladder cancer; MTHFD2, methylenetetrahydrofolate dehydrogenase 2; RT-qPCR, reverse transcription-quantitative PCR; TCGA, The Cancer Genome Atlas; TMA, tissue microarray.

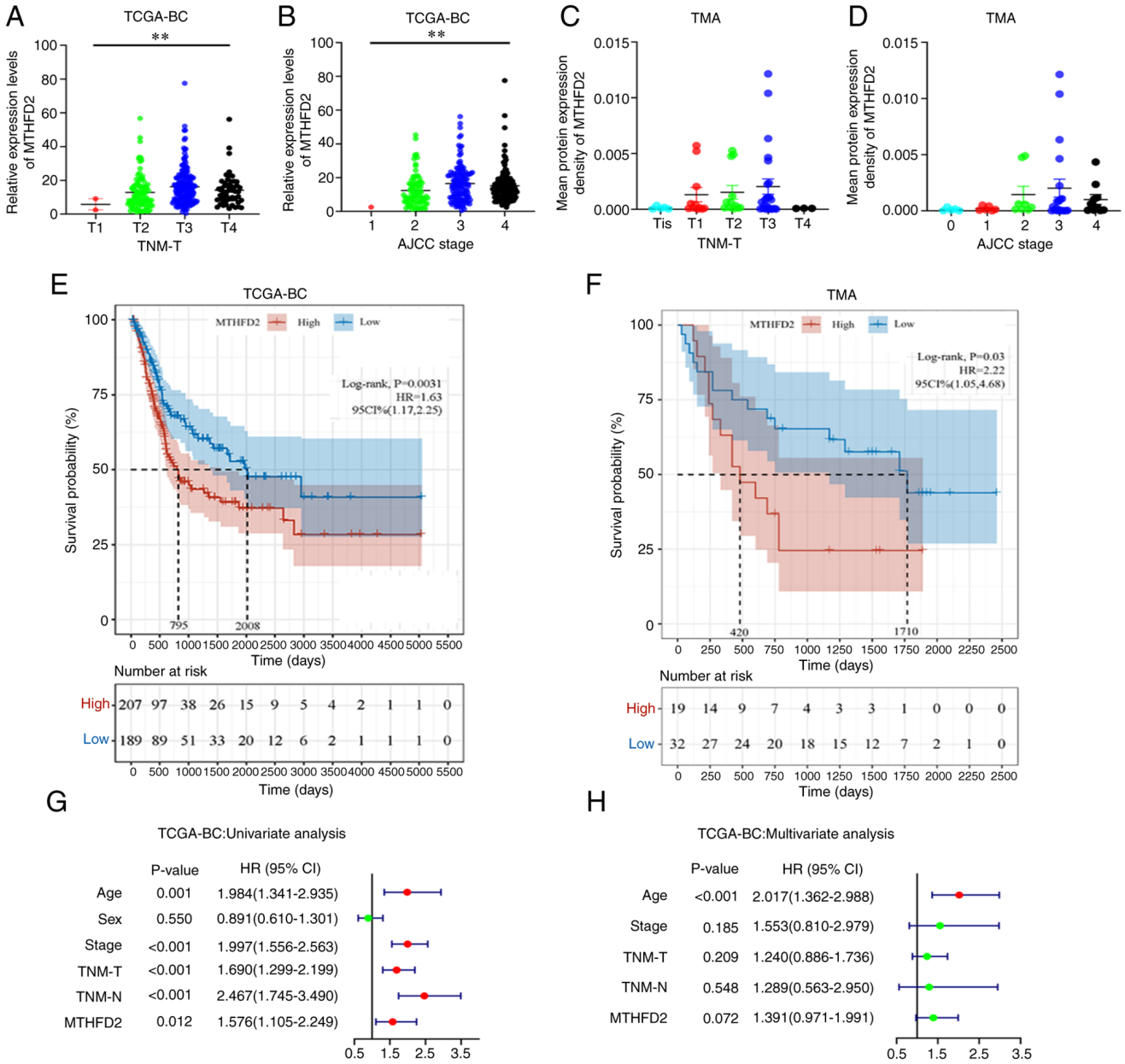

Figure 2. Elevated MTHFD2 expression is associated with a poor prognosis in BC. Association of MTHFD2 expression with (A) TNM-T stage and (B) AJCC stage in TCGA-BC cohort, and (C) TNM-T stage and (D) AJCC stage in TMA cohort. Association of MTHFD2 expression with overall survival in (E) TCGA-BC cohort and (F) TMA cohort. Forest plot of (G) univariate and (H) multivariate Cox regression analysis in TCGA-BC cohort. **P<0.01. AJCC, American Joint Committee on Cancer; BC, bladder cancer; MTHFD2, methylenetetrahydrofolate dehydrogenase 2; TCGA, The Cancer Genome Atlas; TMA, tissue microarray.

CD8 (r=0.29; P=0.02; Fig. 3F) and PD-L1 (r=0.34; P=7.9x10^{-3}; Fig. 3G) expression. Taken together, these results suggested that there is an association between MTHFD2 expression and immune cell infiltration in BC.

MTHFD2 exerts oncogenic effects on BC. To further confirm the function of MTHFD2 in BC, T24 and UMUC3 cell lines with stable knockdown of MTHFD2 expression were constructed. The results of RT-qPCR (Fig. 4A and B) and western blot analysis (Fig. 4C and D) revealed that the expression levels of MTHFD2 were significantly decreased in T24 and UMUC3 cells following lentiviral infection. As the knockdown effect of shRNA2 was better than that of the other shRNAs, it was used for further experiments.

CCK-8 (Fig. 4E) and colony formation (Fig. 4F) assays were performed to detect the effects of MTHFD2 knockdown on the proliferation of T24 and UMUC3 cells. The results revealed that the proliferative ability of T24-shRNA2 and UMUC3-shRNA2 cells was significantly decreased (P<0.05) compared with that in the NC groups. To clarify the mechanism underlying the effects of MTHFD2 on BC proliferation, cell cycle progression and apoptosis were detected following MTHFD2 knockdown by flow cytometry. Through PI detection of the cell cycle, it was revealed that the number of cells in G_1 phase was increased in the T24-shRNA2 and UMUC3-shRNA2 groups, indicating that cells were arrested in the G_0/G_1 phase (Fig. 4G). Furthermore, 7-AAD and Annexin V-APC were used to assess the apoptosis of BC cells;

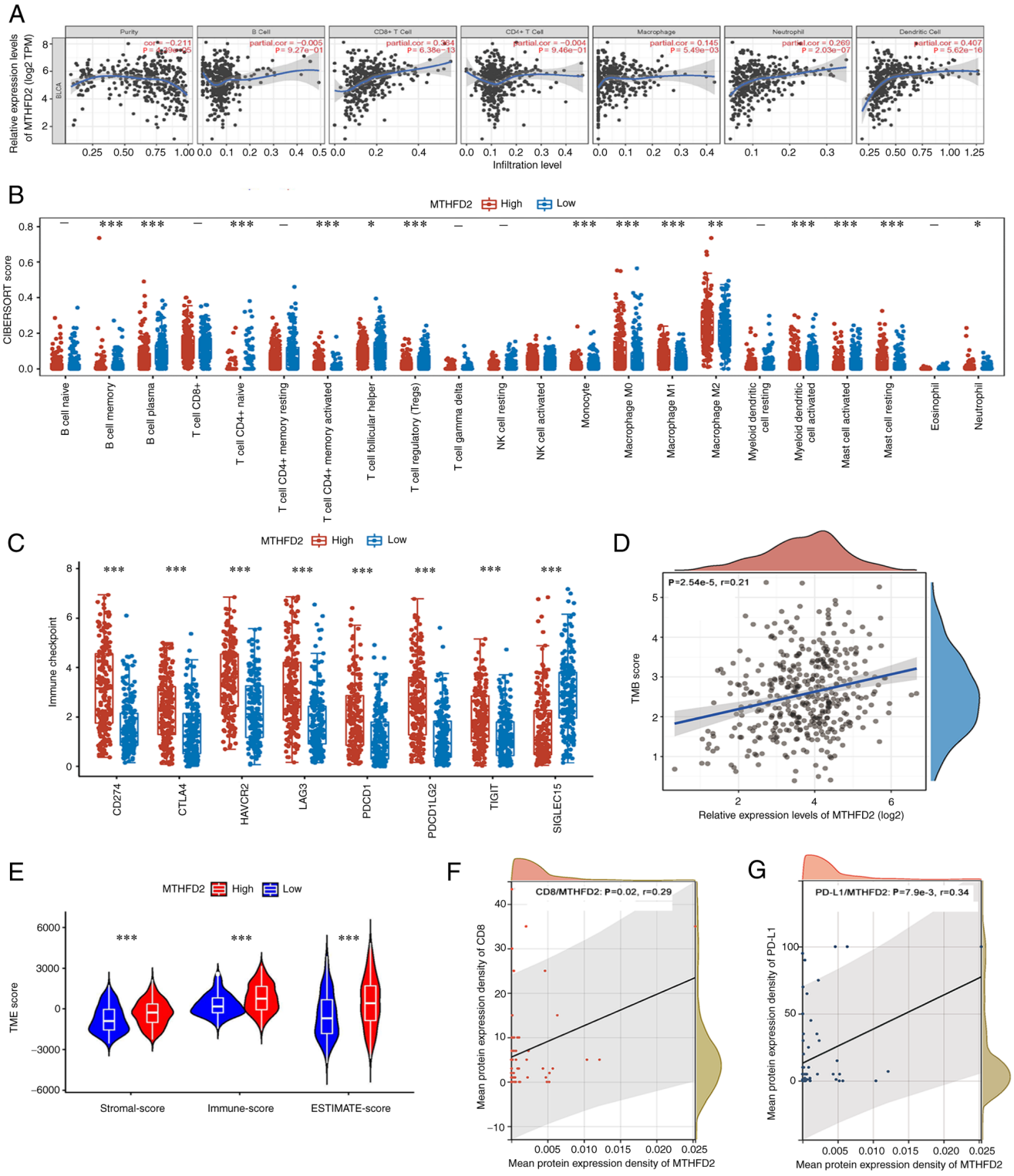

Figure 3. MTHFD2 is associated with immune infiltration in BC. (A) MTHFD2 expression was negatively correlated with tumor purity, and positively correlated with the infiltration of $CD8^+$ T cells, macrophages, neutrophils and dendritic cells in TCGA-BC dataset, as determined by TIMER analysis. (B) Association of MTHFD2 expression with several immune cells in TCGA-BC dataset, as determined using CIBERSORT. (C) MTHFD2 expression was strongly related with the expression of immune checkpoint molecules CD274, CTLA4, HAVCR2, LAG3, PDCD1, PDCD1LG2, TIGIT and SIGLEC15 in TCGA-BC dataset. (D) MTHFD2 expression was significantly positively correlated with TMB in TCGA-BC dataset. (E) Association of MTHFD2 expression with the TME presented as ESTIMATE, Immune and Stromal scores in TCGA-BC dataset. MTHFD2 expression was significantly and positively correlated with (F) CD8 and (G) PD-L1 in TMA. *P<0.05, **P<0.01, ***P<0.001. BC, bladder cancer; MTHFD2, methylenetetrahydrofolate dehydrogenase 2; PD-L1, programmed death-ligand 1; TCGA, The Cancer Genome Atlas; TMA, tissue microarray; TMB, tumor mutational burden; TME, tumor microenvironment.

the results suggested that the number of late apoptotic cells was higher in cells with MTHFD2 knockdown compared with that in the NC groups (Fig. 4H).

Due to the significant association of MTHFD2 with PD-L1 observed in previous analyses, PD-L1 protein expression was examined in T24-shRNA2 cells. As shown in Fig. 4I, upon

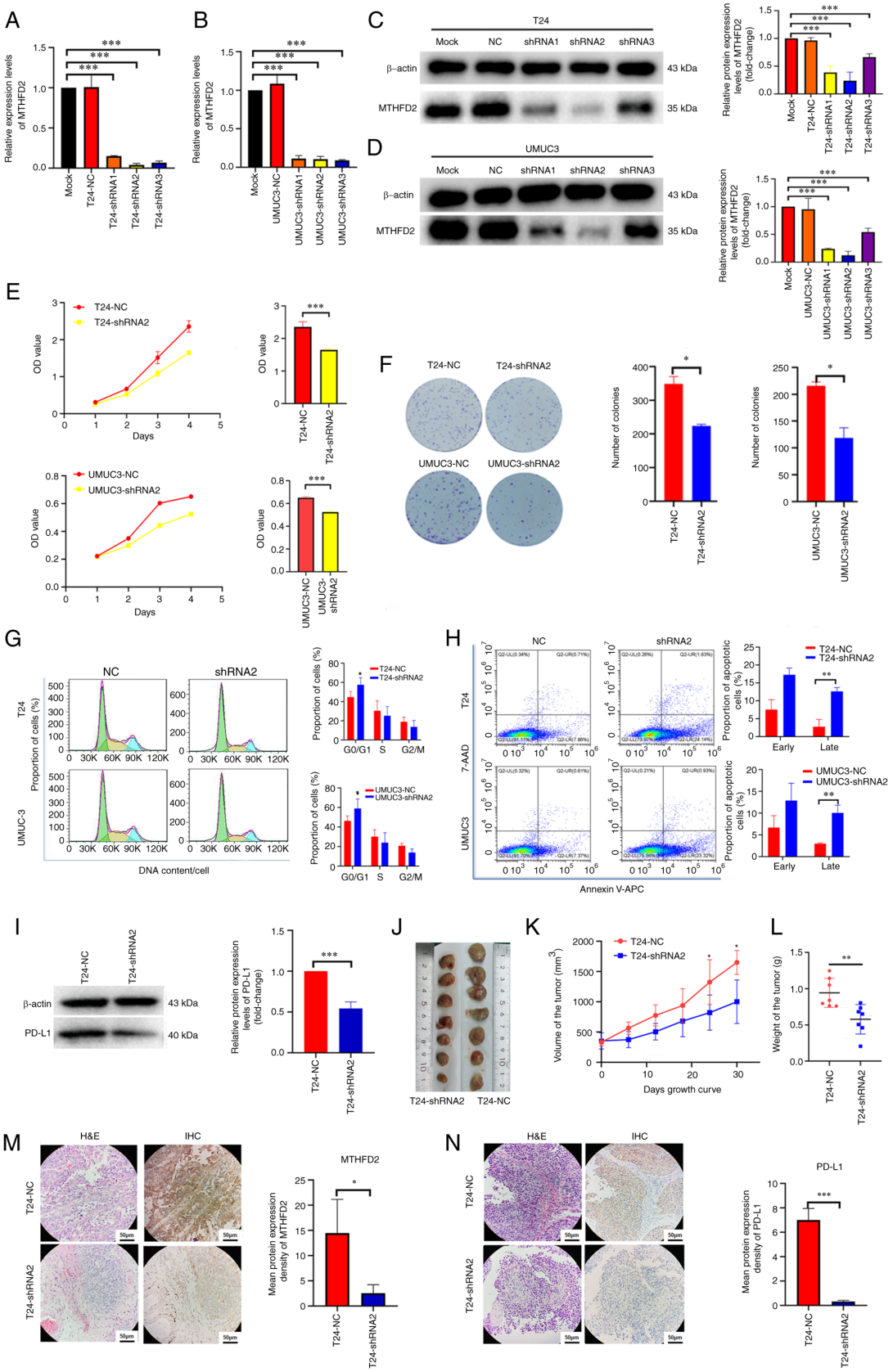

Figure 4. Knockdown of MTHFD2 inhibits the proliferation of bladder cancer cells. The knockdown efficiency of MTHFD2-shRNAs was detected by reverse transcription-qPCR in (A) T24 and (B) UMUC3 cells, and by western blotting in (C) T24 and (D) UMUC3 cells. (E) Cell proliferation was determined by the Cell Counting Kit-8 assay. The bar charts shown the proliferative capacity of cells on day 4. (F) Tumorigenic capacity was determined by colony formation assay. (G) Cell cycle and (H) cell apoptosis were determined by flow cytometry. (I) Expression levels of PD-L1 were determined by western blotting in T24 cells infected with MTHFD2 and NC shRNAs. (J) Images of the subcutaneous tumors formed in the nude mice following injection with T24-shRNA2 and T24-NC cells. (K) Tumor volume and (L) tumor weight were reduced in the T24-shRNA2 group compared with those in the T24-NC group. (M and N) Representative H&E staining, and IHC of (M) MTHFD2 and (N) PD-L1 in tumor xenograft tissues compared between the two groups. *P<0.05, **P<0.01, ***P<0.001 as indicated or vs. T24-shRNA2. 7-AAD, 7-aminoactinomycin D; APC, allophycocyanin; IHC, immunohistochemistry; MTHFD2, methylenetetrahydrofolate dehydrogenase 2; NC, negative control; OD, optical density; PD-L1, programmed death-ligand 1; shRNA, short hairpin RNA; Mock, uninfected T24 or UMUC3 cells.

knockdown of MTHFD2, the expression levels of PD-L1 were also significantly downregulated. These findings were verified *in vivo*. T24-shRNA2 cells were subcutaneously injected into nude mice, and T24-NC cells were used as the NC. As shown in Fig. 4J-L, compared with those in the T24-NC group, the xenografts in the T24-shRNA2 group were significantly smaller and weighed less. Consistent with the results in cell lines, the MTHFD2 and PD-L1 expression levels in xenografts detected via IHC were significantly downregulated in the T24-shRNA2 group (Fig. 4M and N).

Pathway analysis. To identify the signaling pathways regulated by MTHFD2, the transcriptome data of TCGA-BC cohort were analyzed. Using the median MTHFD2 expression as the cut-off value, the cohort was divided into two groups with high or low MTHFD2 expression. As shown in Fig. 5A, 2,319 upregulated and 639 downregulated DEGs were found. 'KEGG' (Fig. 5B and C), 'GO' (Fig. 5D and E) and Hallmark gene sets were used in the 'GSEA', which revealed that the function of MTHFD2 was associated with multiple metabolic pathways and immune regulation, such as 'T-cell activation', 'cytokine production and interactions', as well as 'DNA replication and cell cycle regulation'. In terms of signaling pathways, the PI3K/AKT/mTOR, Myc targets and certain interleukin-regulated pathways were significantly enriched (Fig. 5F and G). For further verification, RNA-seq was used to analyze three replicates of T24-shRNA2 and T24-NC cells. A total of 367 upregulated and 120 downregulated DEGs were found (Fig. 5I). Enrichment analysis revealed numerous terms in the enriched functions and pathways, such as intracellular signal transduction, regulation of molecular function and blood vessel development (Fig. 5J). The PI3K/AKT signaling pathway was also significantly enriched when MTHFD2 was knocked down (Fig. 5K). Using GSVA (single-sample GSEA) analysis, a weak positive correlation was observed between MTHFD2 expression and PI3K/AKT pathway activation (r=0.29; Fig. 5H). The PI3K/AKT signaling pathway was located at the central node in the network constructed using the significantly enriched KEGG pathways (Fig. 5L). Thus, the subsequent experiments focused on this signaling pathway.

Knockdown of MTHFD2 inhibits the proliferation of BC cells through inactivation of the PI3K/AKT signaling pathway. To further confirm the mechanism underlying the effects of MTHFD2 on the proliferation of BC cells, the total and p-levels of PI3K and AKT proteins were detected by western blot analysis, and 740Y-P (an agonist of PI3K) was used to stimulate this signaling pathway. It was observed that the expression levels of p-PI3K and p-AKT were significantly decreased after silencing MTHFD2 in T24 cells, whereas no marked differences in total PI3K and AKT were detected, which resulted in the decreased ratio of p-PI3K/PI3K and p-AKT/AKT (Fig. 6A and B). By contrast, when T24-shRNA2 cells were treated with 740Y-P, the expression levels of p-PI3K/PI3K and p-AKT/AKT were increased in a dose-dependent manner (Fig. 6A). In addition, the change in p-AKT/AKT was not significant (Fig. 6B), which may be due to the high degree of background activation. Subsequently, a series of functional recovery experiments using 740Y-P were conducted. The results demonstrated that the proliferation and colony-forming abilities were inhibited by silencing of MTHFD2 in T24-shRNA2 cells, whereas they were restored following 740Y-P stimulation (Fig. 6C and D). Furthermore, the late apoptosis induced by silencing of MTHFD2 was partially inhibited following 740Y-P stimulation (Fig. 6E). The decrease in PD-L1 expression induced by silencing of MTHFD2 in T24-shRNA2 cells was also partially restored following 740Y-P stimulation (Fig. 6F). These results suggested that MTHFD2 functions in BC in part through the PI3K/AKT signaling pathway.

MTHFD2 may be an effective indicator for chemotherapy and targeted therapy sensitivity of BC. The association between MTHFD2 expression and multiple drug sensitivity (IC_{50}) in BC was predicted using the GDSC database. These drugs analyzed fall into two main categories: i) Those recommended in clinical guidelines for conventional chemotherapy and ii) those targeting the PI3K/AKT signaling pathway. As shown in Fig. 7, there was a negative correlation between MTHFD2 expression and the IC_{50} of conventional chemotherapy drugs, including doxorubicin (r=-0.32; $P=2.33x10^{-11}$; Fig. 7A), cisplatin (r=-0.48; $P=7.39x10^{-25}$; Fig. 7B), methotrexate (r=-0.41; $P=1.68x10^{-17}$; Fig. 7C), mitomycin C (r=-0.13; P=0.012; Fig. 7D), 5-fluorouracil (r=-0.36; $P=6.98x10^{-14}$; Fig. 7E), camptothecin (r=-0.44; $P=4.35x10^{-21}$; Fig. 7F), vinblastine (r=-0.48; $P=4.75x10^{-25}$; Fig. 7G) and gemcitabine (r=-0.43; $P=2.04x10^{-19}$; Fig. 7H). However, the correlations with doxorubicin, mitomycin C and 5-fluorouracil were weak. There was also a weak negative correlation between MTHFD2 expression and the IC_{50} of drugs that target the PI3K/AKT signaling pathway, including A.443554 (r=-0.33; $P=1.73x10^{-11}$; Fig. 7I), PF.4708671 (r=-0.28; $P=8.75x10^{-9}$; Fig. 7J), AZD6482 (r=-0.21; $P=1.51x10^{-5}$; Fig. 7K), TGX221 (r=-0.15; P=0.002; Fig. 7L), PIK-93 (r=-0.20; $P=4.53x10^{-5}$; Fig. 7M) and YM201636 (r=-0.18; $P=2.78x10^{-4}$; Fig. 7O), while a positive correlation was observed with the AKT inhibitor VIII (r=-0.40; $P=6.5x10^{-17}$; Fig. 7N). A negative correlation between MTHFD2 expression and drug sensitivity suggested that MTHFD2 may be an effective indicator for chemotherapy and targeted therapy sensitivity of BC.

Discussion

The treatment of muscle-invasive and metastatic BC has become a focus of research attention, because of its high recurrence and mortality rates. For muscle-invasive BC, radical cystectomy with lymph node dissection remains the recommended treatment. For metastatic BC, cisplatin-based chemotherapy remains the first choice. Perioperative immunotherapy can be offered in a clinical trial setting (3). In the case of distant metastasis, the 5-year survival rate has been reported to be reduced to ~10.2% and the mortality rate has not improved (27). This may be due to the lack of specific therapeutic targets for BC (28). Therefore, it is necessary to identify personalized and precise treatment methods for BC, including exploring the molecular mechanism and identifying novel targets for the treatment of BC (29).

The present study used a combination of bioinformatics analysis and experimental validation to systematically investigate the expression, function and molecular mechanisms involved in the action of MTHFD2 in BC, and analyzed the

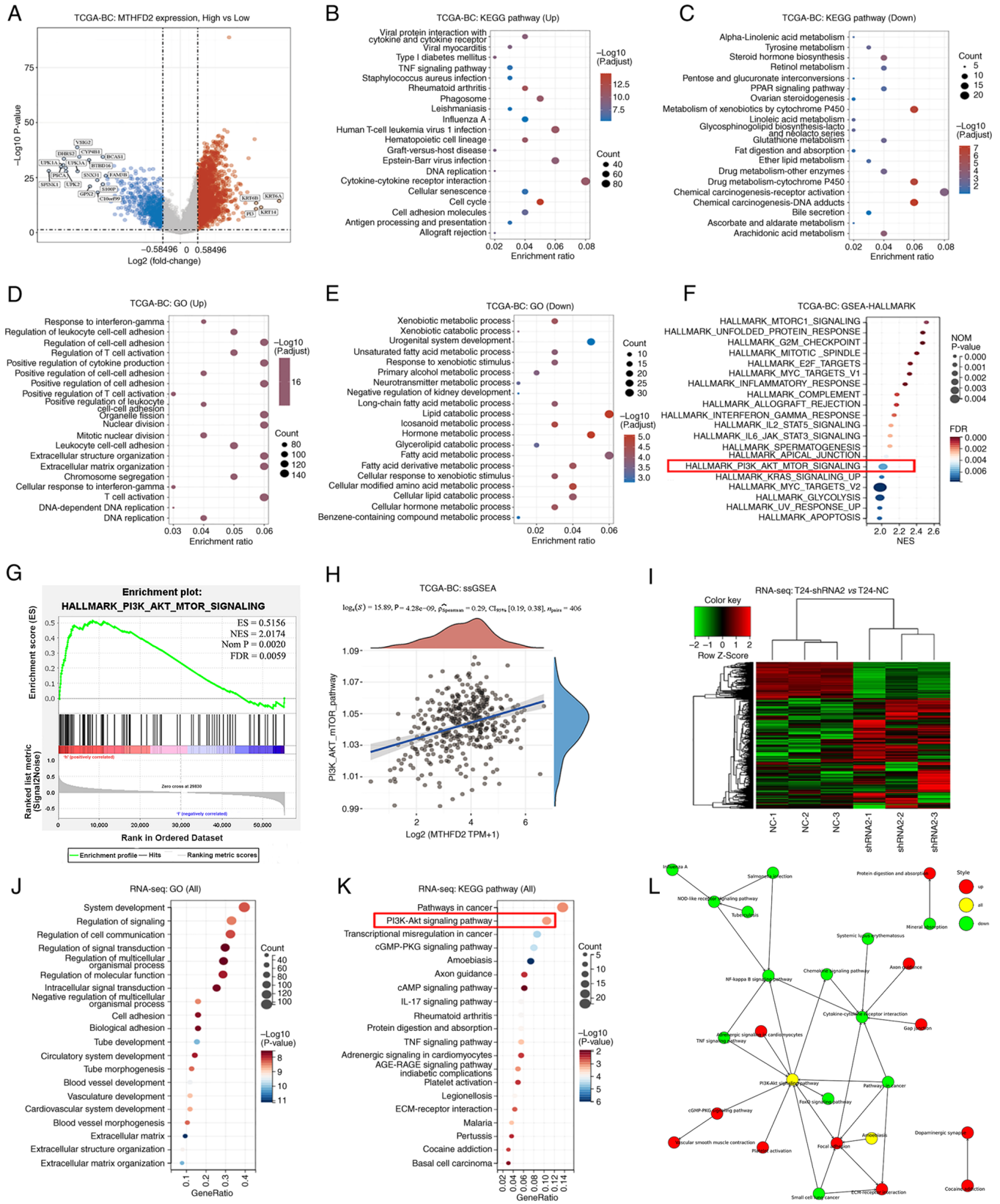

Figure 5. MTHFD2 related pathway analysis in BC. Analyses between patients with low- and high-MTHFD2 expression from TCGA-BC cohort: (A) Volcano plot presents DEGs; red dots indicate upregulated genes, blue dots indicate downregulated genes and grey dots indicate genes with no significant difference. The top 20 enriched KEGG pathways in (B) upregulated DEGs and (C) downregulated DEGs. The top 20 enriched GO functions in (D) upregulated DEGs and (E) downregulated DEGs. (F) Top 20 enriched pathways in GSEA using Hallmark gene sets. (G) Enrichment result of PI3K-AKT-mTOR signaling in GSEA-Hallmark. (H) Correlation between MTHFD2 and PI3K-AKT-mTOR signaling analyzed by ssGSEA. Analyses of RNA-seq data between T24-shRNA2 and T24-NC cells: (I) A heatmappresents DEGs. (J) Top 20 enriched GO functions. (K) Top 20 enriched KEGG pathways. (L) Network of significantly enriched KEGG pathways presented by Cytoscape. BC, bladder cancer; DEG, differentially expressed gene; GO, Gene Ontology; GSEA, Gene Set Enrichment Analysis; KEGG, Kyoto Encyclopedia of Genes and Genomes; MTHFD2, methylenetetrahydrofolate dehydrogenase 2; NC, negative control; RNA-seq, RNA-sequencing; shRNA, short hairpin RNA; ssGSEA, single-sample GSEA; TCGA, The Cancer Genome Atlas.

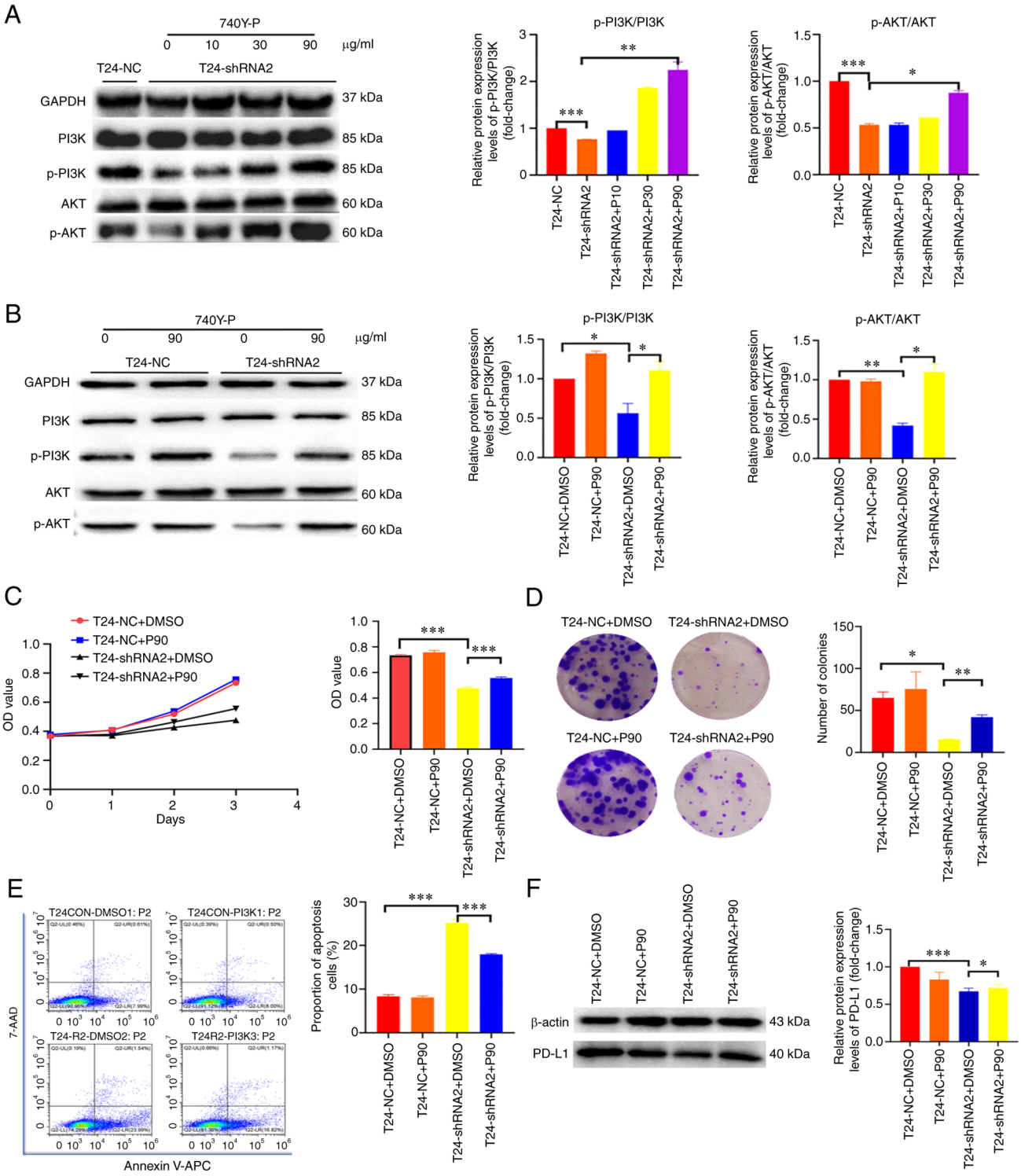

Figure 6. MTHFD2 functions through the PI3K/AKT signaling pathway in bladder cancer. (A) Western blot analysis of the activation status of PI3K/AKT signaling under different concentrations of 740Y-P stimulation in T24-shRNA2 cells. (B) Comparison of the activation status of PI3K/AKT signaling between T24-shRNA2 and T24-NC cells with 740Y-P stimulation. Cell proliferation analyzed by (C) Cell Counting Kit-8 and (D) colony formation assay. The bar charts show the proliferative and colony-forming capacity of cells at day 4 and 14, respectively. (E) Cell apoptosis (sum of early and late apoptotic cells) was analyzed by flow cytometry in T24-shRNA2 and T24-NC cells with 740Y-P stimulation. (F) Western blot analysis of PD-L1 expression in T24-shRNA2 and T24-NC cells with 740Y-P stimulation. *P<0.05, **P<0.01, ***P<0.001. 7-AAD, 7-aminoactinomycin D; APC, allophycocyanin; IHC, immunohistochemistry; NC, negative control; OD, optical density; p-, phosphorylated; PD-L1, programmed death-ligand 1; shRNA, short hairpin RNA.

association between its expression and patient prognosis and immune infiltration, with a focus on its association with PD-L1. Through analysis of public database-derived expression data and experimental validation, the present study confirmed the specific upregulation of MTHFD2 expression and its association with poor prognosis in BC, which is consistent with its expression in a variety of tumors (9-13), including BC in other studies (17,18). Unlike other bioinformatics reports, the current study not only performed bioinformatics analysis of data in public databases, but also validated the results

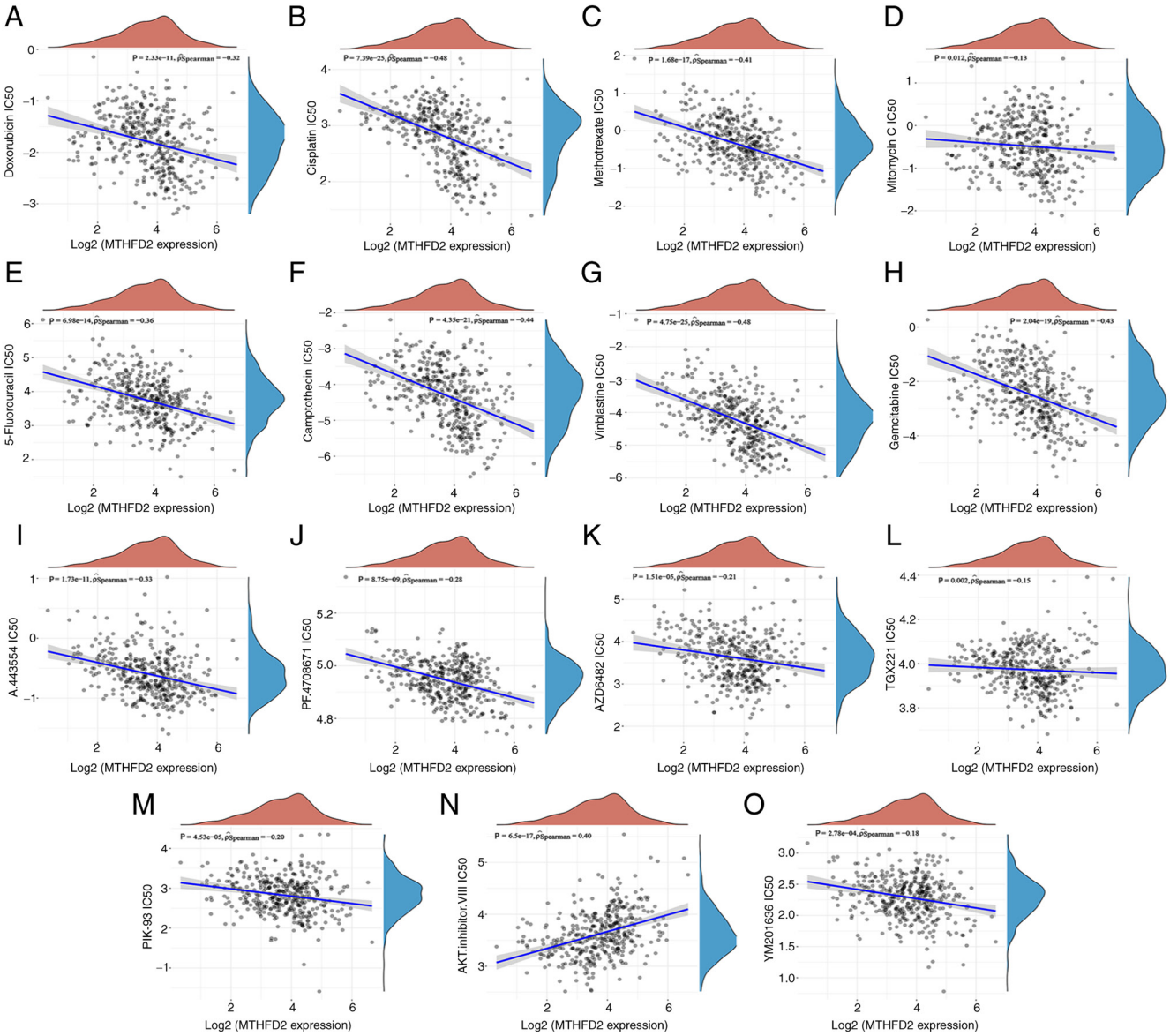

Figure 7. Prediction of association between MTHFD2 expression and drug sensitivity in GDSC. The correlation between MTHFD2 expression and the IC_{50} of conventional chemotherapy drugs, including (A) doxorubicin, (B) cisplatin, (C) methotrexate, (D) mitomycin C, (E) 5-fluorouracil, (F) camptothecin, (G) vinblastine and (H) gemcitabine, and PI3K/AKT pathway targeting drugs, including (I) A.443554, (J) PF.4708671, (K) AZD6482, (L) TGX221, (M) PIK-93, (N) AKT.inhibitor.VIII and (O) YM201636. IC_{50}, half maximal inhibitory concentration; MTHFD2, methylenetetrahydrofolate dehydrogenase 2.

with commercial TMAs and patient samples collected at our hospital, which ensures the reliability of the conclusions.

In a preclinical experiment (17), MTHFD2 was revealed to be upregulated in patients with metastatic urothelial cancer and Mariathasan *et al* (30) reported that advanced BC had a good response to an anti-PD-L1 agent (atezolizumab). Therefore, the present study evaluated the association between MTHFD2 and biomarkers of immune checkpoint therapy. The correlation between MTHFD2 and immune infiltration level, TMB, immune checkpoint molecules and TME were investigated. Notably, MTHFD2 was significantly correlated with all of these markers, suggesting its potential as a new marker for immune checkpoint therapy. The present study also identified certain differences in the immune cell association results between TIMER and CIBERSORT in immune cell infiltration analysis. This may be due to the difference in the design of the two algorithms; however, it does not affect the conclusion that MTHFD2 is highly associated with immune cell infiltration in BC.

As one of the key enzymes involved in folate metabolism, MTHFD2 serves a key role in metabolic reprogramming (31), which fulfills the cellular bioenergetic and biosynthetic needs that occur in both cancer and immune cells inside the tumor mass, and may influence their interaction (32). MTHFD2 has been reported to be a metabolic checkpoint that controls the fate and function of effector and regulatory T cells (33). Therefore, mechanistically, the involvement of MTHFD2 in tumor immunity is understandable.

The association between MTHFD2 and PD-L1 was also investigated in the present study, and it was revealed that MTHFD2 was positively correlated with PD-L1 expression in BC tissues, and knockdown of MTHFD2 in BC cells resulted in the downregulation of PD-L1 expression. In a subsequent mechanistic analysis, it was demonstrated that MTHFD2

regulated PD-L1 expression through the PI3K/AKT signaling pathway. This finding was consistent with a recent report in pancreatic cancer (34).

The current study also predicted the association between MTHFD2 and chemotherapeutic drug sensitivity using the GDSC database. In addition, MTHFD2 expression was also correlated with the IC_{50} of various PI3K/AKT signaling pathway-targeting drugs, which was consistent with the results of mechanistic analysis.

There are certain limitations in the present study. First, due to the small number of TMA and self-sampled cases, analyses such as Cox regression may be largely affected by bias. Second, due to financial and time constraints, the mechanism by which MTHFD2 induces immune escape in bladder cancer via regulating immune-related molecules has not been determined, and it is our intention to investigate it in depth in subsequent studies.

In conclusion, the current study used a combination of bioinformatics analysis and experimental validation to investigate the expression, function and molecular mechanisms of MTHFD2 in BC, and analyzed the association between its expression and patient prognosis and immune infiltration, with a focus on its association with PD-L1. The present findings suggested that MTHFD2 could be a promising marker and therapeutic target of chemotherapy and immunotherapy for BC.

Acknowledgments

The authors would like to thank Professor Weidong Li and Professor Xiaoyuan Xu for their help in the process of experimental design and operation in the Jiangxi Provincial Key Lab of System Biomedicine (Jiangxi, China).

Funding

This study was supported by the National Natural Science Foundation of P.R. China (grant nos. 82260511, 81960512 and 81760457), Jiangxi Provincial 'Double Thousand Plan' Fund Project (grant no. jxsq2019201027), the Key Project of Natural Science Foundation of Jiangxi Province (grant no. 20212ACB206013), and the Youth Project of Natural Science Foundation of Jiangxi Province (grant no. 20212BAB216037).

Availability of data and materials

The RNA-seq data generated and/or analyzed during the current study are available in the Gene Expression Omnibus repository under accession number GSE217785 (https://www.ncbi.nlm.nih.gov/geo/query/acc.cgi?acc=GSE217785). All other datasets used and/or analyzed during the current study are available from the corresponding author on reasonable request.

Authors' contributions

BF and WZ designed the project and revised the manuscript. XD and XL performed the experiments, collected the data and wrote the manuscript. JL and BH assisted with the experiments and analyzed the data. XD and XL confirm the authenticity of all the raw data. All authors read and approved the final manuscript.

Ethics approval and consent to participate

The present study was approved by the Research Ethics Committee of the First Affiliated Hospital of Nanchang University [approval no. (2021)51] and the Animal Care and Use Committees of Nanchang University [institutional approval number for lab animal studies: SYXK (Gan) 2015-0001] and were performed in accordance with the ethical standards laid down in The Declaration of Helsinki. The present study was conducted with written informed consent from all of the patients.

Patient consent for publication

Not applicable.

Competing interests

The authors declare that they have no competing interests.

References

1. Sung H, Ferlay J, Siegel RL, Laversanne M, Soerjomataram I, Jemal A and Bray F: Global cancer statistics 2020: GLOBOCAN estimates of incidence and mortality worldwide for 36 cancers in 185 countries. CA Cancer J Clin 71: 209-249, 2021.
2. Schmitz-Drager BJ, Droller M, Lokeshwar VB, Lotan Y, Hudson MA, van Rhijn BW, Marberger MJ, Fradet Y, Hemstreet GP, Malmstrom PU, *et al*: Molecular markers for bladder cancer screening, early diagnosis, and surveillance: The WHO/ICUD consensus. Urol Int 94: 1-24, 2015.
3. Witjes JA, Bruins HM, Cathomas R, Compérat EM, Cowan NC, Gakis G, Hernández V, Espinós EL, Lorch A, Neuzillet Y, *et al*: European association of urology guidelines on muscle-invasive and metastatic bladder cancer: Summary of the 2020 guidelines. Eur Urol 79: 82-104, 2021.
4. Lopez-Beltran A, Cimadamore A, Blanca A, Massari F, Vau N, Scarpelli M, Cheng L and Montironi R: Immune checkpoint inhibitors for the treatment of bladder cancer. Cancers (Basel) 13: 131, 2021.
5. Balar AV, Galsky MD, Rosenberg JE, Powles T, Petrylak DP, Bellmunt J, Loriot Y, Necchi A, Hoffman-Censits J, Perez-Gracia JL, *et al*: Atezolizumab as first-line treatment in cisplatin-ineligible patients with locally advanced and metastatic urothelial carcinoma: A single-arm, multicentre, phase 2 trial. Lancet 389: 67-76, 2017.
6. Stenehjem DD, Tran D, Nkrumah MA and Gupta S: PD1/PDL1 inhibitors for the treatment of advanced urothelial bladder cancer. Onco Targets Ther 11: 5973-5989, 2018.
7. Mejia NR and MacKenzie RE: NAD-dependent methylenetetrahydrofolate dehydrogenase is expressed by immortal cells. J Biol Chem 260: 14616-14620, 1985.
8. Nilsson R, Jain M, Madhusudhan N, Sheppard NG, Strittmatter L, Kampf C, Huang J, Asplund A and Mootha VK: Metabolic enzyme expression highlights a key role for MTHFD2 and the mitochondrial folate pathway in cancer. Nat Commun 5: 3128, 2014.
9. Cui X, Su H, Yang J, Wu X, Huo K, Jing X and Zhang S: Up-regulation of MTHFD2 is associated with clinicopathological characteristics and poor survival in ovarian cancer, possibly by regulating MOB1A signaling. J Ovarian Res 15: 23, 2022.
10. Ju HQ, Lu YX, Chen DL, Zuo ZX, Liu ZX, Wu QN, Mo HY, Wang ZX, Wang DS, Pu HY, *et al*: Modulation of redox homeostasis by inhibition of MTHFD2 in colorectal cancer: Mechanisms and therapeutic implications. J Natl Cancer Inst 111: 584-596, 2019.
11. Lin H, Huang B, Wang H, Liu X, Hong Y, Qiu S and Zheng J: MTHFD2 overexpression predicts poor prognosis in renal cell carcinoma and is associated with cell proliferation and vimentin-modulated migration and invasion. Cell Physiol Biochem 51: 991-1000, 2018.
12. Liu F, Liu Y, He C, Tao L, He X, Song H and Zhang G: Increased MTHFD2 expression is associated with poor prognosis in breast cancer. Tumour Biol 35: 8685-8690, 2014.

13. Liu X, Huang Y, Jiang C, Ou H, Guo B, Liao H, Li X and Yang D: Methylenetetrahydrofolate dehydrogenase 2 overexpression is associated with tumor aggressiveness and poor prognosis in hepatocellular carcinoma. Dig Liver Dis 48: 953-960, 2016.
14. Huang J, Qin Y, Lin C, Huang X and Zhang F: MTHFD2 facilitates breast cancer cell proliferation via the AKT signaling pathway. Exp Ther Med 22: 703, 2021.
15. Wei Y, Liu P, Li Q, Du J, Chen Y, Wang Y, Shi H, Wang Y, Zhang H, Xue W, *et al*: The effect of MTHFD2 on the proliferation and migration of colorectal cancer cell lines. Onco Targets Ther 12: 6361-6370, 2019.
16. Shi Y, Xu Y, Yao J, Yan C, Su H, Zhang X, Chen E and Ying K: MTHFD2 promotes tumorigenesis and metastasis in lung adenocarcinoma by regulating AKT/GSK-3β/β-catenin signalling. J Cell Mol Med 25: 7013-7027, 2021.
17. Liu X, Liu S, Piao C, Zhang Z, Zhang X, Jiang Y and Kong C: Non-metabolic function of MTHFD2 activates CDK2 in bladder cancer. Cancer Sci 112: 4909-4919, 2021.
18. Zhu L, Liu X, Zhang W, Hu H, Wang Q and Xu K: MTHFD2 is a potential oncogene for its strong association with poor prognosis and high level of immune infiltrates in urothelial carcinomas of bladder. BMC Cancer 22: 556, 2022.
19. Dillies MA, Rau A, Aubert J, Hennequet-Antier C, Jeanmougin M, Servant N, Keime C, Marot G, Castel D, Estelle J, *et al*: A comprehensive evaluation of normalization methods for Illumina high-throughput RNA sequencing data analysis. Brief Bioinform 14: 671-683, 2013.
20. Li T, Fan J, Wang B, Traugh N, Chen Q, Liu JS, Li B and Liu XS: TIMER: A web server for comprehensive analysis of tumor-infiltrating immune cells. Cancer Res 77: e108-e110, 2017.
21. Shannon P, Markiel A, Ozier O, Baliga NS, Wang JT, Ramage D, Amin N, Schwikowski B and Ideker T: Cytoscape: A software environment for integrated models of biomolecular interaction networks. Genome Res 13: 2498-2504, 2003.
22. Liu X, Xu X, Deng W, Huang M, Wu Y, Zhou Z, Zhu K, Wang Y, Cheng X, Zhou X, *et al*: CCL18 enhances migration, invasion and EMT by binding CCR8 in bladder cancer cells. Mol Med Rep 19: 1678-1686, 2019.
23. Livak KJ and Schmittgen TD: Analysis of relative gene expression data using real-time quantitative PCR and the 2(-Delta Delta C(T)) method. Methods 25: 402-408, 2001.
24. Kim D, Langmead B and Salzberg SL: HISAT: A fast spliced aligner with low memory requirements. Nat Methods 12: 357-360, 2015.
25. Anders S, Pyl PT and Huber W: HTSeq-a python framework to work with high-throughput sequencing data. Bioinformatics 31: 166-169, 2015.
26. Li Y, Ma Y, Wu Z, Zeng F, Song B, Zhang Y, Li J, Lui S and Wu M: Tumor mutational burden predicting the efficacy of immune checkpoint inhibitors in colorectal cancer: A systematic review and meta-analysis. Front Immunol 12: 751407, 2021.
27. Grayson M: Bladder cancer. Nature 551: S33, 2017.
28. Hurst CD, Alder O, Platt FM, Droop A, Stead LF, Burns JE, Burghel GJ, Jain S, Klimczak LJ, Lindsay H, *et al*: Genomic subtypes of non-invasive bladder cancer with distinct metabolic profile and female gender bias in KDM6A mutation frequency. Cancer Cell 32: 701-715 e707, 2017.
29. Kobayashi T, Owczarek TB, McKiernan JM and Abate-Shen C: Modelling bladder cancer in mice: Opportunities and challenges. Nat Rev Cancer 15: 42-54, 2015.
30. Mariathasan S, Turley SJ, Nickles D, Castiglioni A, Yuen K, Wang Y, Kadel EE III, Koeppen H, Astarita JL, Cubas R, *et al*: TGFβ attenuates tumour response to PD-L1 blockade by contributing to exclusion of T cells. Nature 554: 544-548, 2018.
31. Ducker GS, Chen L, Morscher RJ, Ghergurovich JM, Esposito M, Teng X, Kang Y and Rabinowitz JD: Reversal of cytosolic one-carbon flux compensates for loss of the mitochondrial folate pathway. Cell Metab 23: 1140-1153, 2016.
32. Singer K, Cheng WC, Kreutz M, Ho PC and Siska PJ: Immunometabolism in cancer at a glance. Dis Model Mech 11: dmm034272, 2018.
33. Sugiura A, Andrejeva G, Voss K, Heintzman DR, Xu X, Madden MZ, Ye X, Beier KL, Chowdhury NU, Wolf MM, *et al*: MTHFD2 is a metabolic checkpoint controlling effector and regulatory T cell fate and function. Immunity 55: 65-81 e69, 2022.
34. Shang M, Yang H, Yang R, Chen T, Fu Y, Li Y, Fang X, Zhang K, Zhang J, Li H, *et al*: The folate cycle enzyme MTHFD2 induces cancer immune evasion through PD-L1 up-regulation. Nat Commun 12: 1940, 2021.